Dalton Transactions

ROYAL SOCIETY OF CHEMISTRY

PAPER

View Article Online
View Journal | View Issue

Cite this: *Dalton Trans.*, 2023, **52**, 12390

A new family of luminescent $[Pt(pbt)_2(C_6F_5)L]^{n+}$ (n = 1, 0) complexes: synthesis, optical and cytotoxic studies†

David Gómez de Segura,[a] Nora Giménez,[a] David Rincón-Montón,[a] M. Teresa Moreno, *[a] José G. Pichel,[b,c] Icíar P. López*[b] and Elena Lalinde *[a]

Given the widely recognized bioactivity of 2-arylbenzothiazoles against tumor cells, we have designed a new family of luminescent heteroleptic pentafluorophenyl-bis(2-phenylbenzothiazolyl) Pt^{IV} derivatives, *fac*-$[Pt(pbt)_2(C_6F_5)L]^{n+}$ (n = 1, 0) [L = 4-Mepy **1**, 4-pyridylbenzothiazole (**pybt**) **2**, 4,4′-bipyridine (4,4′-bpy) **3**, 1,2-bis-(4-pyridyl)ethylene (bpe) **4** (*E*/*Z* ratio: 90/10), 1,4-bis-(pyridyl)butadiyne (bpyb) **5**, trifluoroacetate ($^-OCOCF_3$) **6**] and a dinuclear complex $[\{Pt(pbt)_2(C_6F_5)\}_2(\mu\text{-bpyb})](PF_6)_2$ **7**, in which the *trans* ligand to the metalated C-(pbt) was varied to modify the optical properties and lipophilicity. Their photophysical properties were systematically studied through experimental and theoretical investigations, which were strongly dependent on the identity of the N-bonded ligand. Thus, complexes **1**, **3** and **6** display, in different media, emission from the triplet excited states of primarily intraligand ^{3}ILCT nature localized on the pbt ligand, while the emissions of **2**, **5** and **7** were ascribed to a mixture of close ^{3}IL′(N donor)/^{3}ILCT (pbt) excited states, as supported by lifetime measurements and theoretical calculations. Irradiation of the initial *E*/*Z* mixture of **4** (15 min) led to a steady state composed of roughly 1 : 1.15 (*E* : *Z*) and this complex was not emissive at room temperature due to an enhanced intramolecular *E* to *Z* isomerization process of the 1,2-bis-(4-pyridyl)ethylene ligand. Complexes **1–3** and **6** showed excellent quantum yields for the generation of singlet oxygen in aerated MeCN solution with the values of $\phi(^1O_2)$ ranging from 0.66 to 0.86 using phenalenone as a reference. Cationic complexes **1–3** exhibited remarkable efficacy in the nanomolar range against A549 (lung carcinoma) and HeLa (cervix carcinoma) cell lines with notable selectivity relative to the non-tumorigenic BEAS-2B (bronchial epithelium) cells. In the A549 cell line, the neutral complex **6** showed low cytotoxicity (IC_{50}: 29.40 μM) and high photocytotoxicity (IC_{50}: 5.75) when cells were irradiated with blue light for 15 min. These complexes do not show evidence of DNA interaction.

Received 7th June 2023,
Accepted 3rd August 2023

DOI: 10.1039/d3dt01759a

rsc.li/dalton

Introduction

Luminescent complexes based on organic chromophores have attracted great interest due to their wide range of potential applications in fields such as photocatalysis,[1] biological sensing,[2] photosensitizers in medicinal chemistry[3] and optoelectronic devices.[4] In particular, d^6 (Ru^{II}, Os^{II}, and Ir^{III})[4c,5] and d^8 (Pt^{II})[6] cyclometalated compounds have been extensively studied due to their ability to promote large spin–orbit coupling in the organic chromophore upon photoexcitation. This leads to fast singlet–triplet intersystem crossing (ISC) between singlet and triplet manifolds, giving rise to potentially emissive low-lying triplet excited states of different characters, including ^{3}MLCT, ^{3}LC ($\pi\pi^*$) or ^{3}LC/^{3}MLCT, and ^{3}LLCT/^{3}MLCT mixtures, depending on the ligands and the electronic density of the metal involved. The selection and/or functionalization of the cyclometalated group and/or the auxiliary ligands are typical approaches for a facile modification of luminescence properties (λ_{em}, ϕ), thus widening the diversity of potential applications. In this framework, cyclometalated complexes of metal ions such as d^6 (Pt^{IV})[7] or d^8 (Pd^{II} [8] or Au^{III} [9]) have received considerably less attention than the related

[a]*Departamento de Química-Centro de Síntesis Química de La Rioja (CISQ), Universidad de La Rioja, 26006 Logroño, Spain. E-mail: elena.lalinde@unirioja.es, teresa.moreno@unirioja.es*
[b]*Lung Cancer and Respiratory Diseases Unit (CIBIR), Fundación Rioja Salud, 26006 Logroño, Spain. E-mail: iplgarcia@riojasalud.es*
[c]*Spanish Biomedical Research Networking Centre in Respiratory Diseases (CIBERES), ISCIII, E-28029 Madrid, Spain. https://www.ciberes.org*

†Electronic supplementary information (ESI) available: Experimental section, characterization of complexes (NMR spectra and crystal data), photophysical properties and computational details. CCDC 2267807–2267809. For ESI and crystallographic data in CIF or other electronic format see DOI: https://doi.org/10.1039/d3dt01759a

isoelectronic octahedral d^6 Ir^{III} or square planar d^8 Pt^{II} systems, likely due to the highly electrophilic nature of these metal ions. This decreases the metal orbital involvement in the low-lying excited state and also stabilizes the d–d metal centred (MC) states, facilitating luminescence quenching at room temperature through thermally activated access to non-radiative d–d states, which compete with the typical emissive intra-ligand (^{3}LC, ^{3}ILCT) or ligand-to-ligand charge transfer (^{3}LLCT) transitions.[10] Among these metals, homo- and heteroleptic bis- and tris(cyclometalated) Pt^{IV} complexes have been successfully investigated by the research group of González-Herrero,[7h–o,11] our laboratory,[12] and others.[13] In general, these complexes exhibit long-lived and easily tuned emissions from essentially ligand-centred triplet excited states (^{3}LC), with a very low contribution of metal-to-ligand charge-transfer (MLCT), which makes them potential candidates for the development of photoinduced systems such as $^1O_2$ sensitizers, photocatalysts and sensors.

On the other hand, since the serendipitous finding of the anticancer activity of cisplatin, the search for new designed Pt and other transition metal (Au,[14] Pd,[15] Ru,[16] and Ir[2,17])-based compounds including multimetallic systems,[18] has contributed to the development of new promising anticancer drugs, in many cases with unique anticancer mechanisms.[19] In Pt chemistry, libraries of antiproliferative Pt complexes have been investigated but only a few of them (carboplatin, oxaliplatin, heptaplatin, lobaplatin, and nedaplatin) have entered clinical use.[20] The cytotoxicity of these drugs is mainly based on the formation of intrastrand cross-links with guanine residues, triggering the inhibition of DNA transcription and apoptosis of cancer cells. To reduce adverse side-effects, circumvent acquired resistance and/or increase selectivity, research has focused on the study of new Pt and other transition metal-based compounds[21] and also on the development of novel approaches[22] such as photodynamic therapy,[23] encapsulation of drugs into delivery systems[24] and targeted and immunological therapies.[25] In recent years, octahedral d^6 Pt^{IV} complexes have emerged as attractive prodrugs of existing clinical Pt^{II} compounds, as these complexes are kinetically stable under physiological conditions being activated by reduction with ascorbic acid or glutathione, preferentially in cancer cells.[26] During this process, they release axial ligands and form their related cytotoxic Pt^{II} counterparts. By incorporation at the axial sites of other biologically active molecules, these Pt^{IV} complexes behave as multi-acting targets capable of releasing various antiproliferative molecules inside the tumour cell, thus modulating the pharmacologic action of the Pt^{II} drug.[27]

The above-mentioned cyclometalated luminescent complexes represent another important growing class of compounds with potential clinical significance. These complexes are excellent probes for cellular imaging or as new trackable or photoactivatable anticancer drugs, acting as multifunctional theranostic systems. Much effort has been devoted to d^6 (Ir^{III}, Ru^{II})[3a,28] and d^8 (Pt^{II} and Au^{III})[29] cyclometalated complexes, which often elicit their activity through different mechanisms from that of cisplatin or trigger their efficiency by increasing reactive oxygen species (ROS) upon photoexcitation.[30] Indeed, some cyclometalated complexes are found in the cytoplasm and do not reach the nucleus.[31] However, despite the increasing importance of Pt^{IV}-based complexes as prodrugs in anticancer therapeutics,[32] reports on the biological activity of related luminescent cycloplatinated Pt^{IV} derivatives remain sparse.[33]

Given the wide applicability of benzothiazole in medicinal chemistry[34] and as a continuation of our ongoing interest in the biological activity of 2-arylbenzothiazol-based cycloplatinated complexes,[35] in this work we designed bis(cyclometalated) Pt^{IV} compounds featuring a *fac*-$Pt(pbt)_2(C_6F_5)$ framework. In detail, we present the synthesis and optical properties of new mononuclear cationic *fac*-$[Pt(pbt)_2(C_6F_5)(L)](PF_6)$ [L = 4-Mepy (**1**), **pybt** (**2**), 4,4′-bpy (**3**), bpe (**4**), bpyb (**5**)] and neutral *fac*-$[Pt(pbt)_2(C_6F_5)(OCOCF_3)]$ (**6**) pentafluorophenyl-bis(cyclometalated) Pt^{IV} compounds and a dinuclear complex $[\{Pt(pbt)_2(C_6F_5)\}_2(\mu\text{-bpyb})](PF_6)_2$ (**7**), in which the *trans* ligand to the metalated C-(pbt) is varied to modify the optical properties and lipophilicity. Computational studies based on density functional theory (DFT) and time-dependent DFT (TD-DFT) were also performed to deepen the understanding of their excited state properties. Complexes **1–3** showed *in vitro* cytotoxicity against human tumour A549 (lung carcinoma) and HeLa (cervix carcinoma) cell lines with notable selectivity with respect to the non-tumorigenic BEAS-2B (bronchial epithelium) cells and complex **6** exhibited highly efficient photoinduced cytotoxicity upon short light irradiation by $^1O_2$ generation. Finally, we evaluated a plausible mechanism of action of these complexes by analysing their interaction with DNA.

Results and discussion

Synthesis and characterization

The synthetic pathway of the complexes presented in this work is summarized in Scheme 1. Cationic bis(cycloplatinated) Pt^{IV} complexes, *fac*-$[Pt(pbt)_2(C_6F_5)(L)](PF_6)$ **1–5**, were prepared by employing a chloride derivative *fac*-$[Pt(pbt)_2(C_6F_5)Cl]$ as the precursor, previously synthesized in our group.[12a] The displacement of the chloride by the corresponding N-donor ligand required drastic conditions and took place at reflux in 1,2-dicloroethane with an excess of the corresponding N-donor ligand and $TlPF_6$ (2 equiv.) as well as $K(ClO_4)$ (excess) to facilitate the abstraction of Cl^-. The reaction times to form the corresponding cationic complexes *fac*-$[Pt(pbt)_2(C_6F_5)(L)](PF_6)$ [L = 4-Mepy (**1**), **pybt** (**2**), 4,4′-bpy (**3**), bpe (**4**), bpyb (**5**)] varied between 5 and 15 h, and the progress was monitored by $^{19}F\{^1H\}$ NMR spectroscopy (Fig. S1–S7†). The reaction with the *trans*-bpe ligand was carried out protected from light and even under these conditions the final solid contained the ligand in a mixture of the $E:Z$ ratio (90 : 10) (see Fig. S8†). In the case of the synthesis of 1,4-bis(4-pyridyl)butadiyne complex **5**, was always impurified by an small amount of the bimetallic derivative *fac*-$[\{Pt(pbt)_2(C_6F_5)\}_2(\mu\text{-bpyb})](PF_6)_2$ (**7**) featuring a 1,4-bis(4-pyridyl)butadiyne ligand acting as a symmetrical bridging

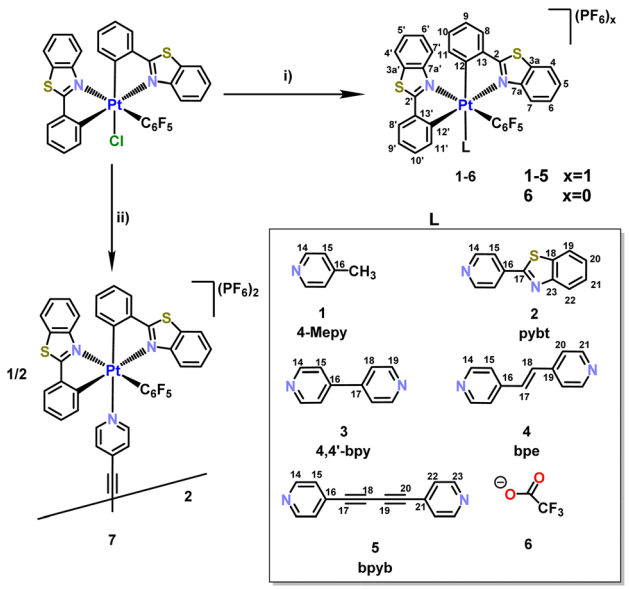

Scheme 1 Labelling; reagents and conditions: (i) L (3 equiv. of **1**, **2**, **4** and **5**; 5 equiv. of **3**); $TlPF_6$ (2 equiv.); $KClO_4$ (exc.); $C_2H_4Cl_2$; reflux (5 h for **1**; 15 h for **2**, **3** and **5**; 10 h for **4**) and for **6** $AgCF_3CO_2$ (1 equiv.); acetone; reflux (6 h). (ii) bpyb (0.5 equiv.); $TlPF_6$ (3 equiv.); $KClO_4$ (exc.); $C_2H_4Cl_2$, reflux 6 h.

ligand of two Pt^{IV} $\{Pt(pbt)_2(C_6F_5)\}$ units. Complex **7** was alternatively obtained in high yield by using a Pt : bpyb 1 : 0.5 molar ratio. The neutral complex *fac*-$[Pt(pbt)_2(C_6F_5)(OCOCF_3)]$ (**6**), containing an O-donor trifluoroacetate ligand *trans* to a metalated C-pbt, was generated by a reaction at reflux of the chloride precursor with a stoichiometric amount of $AgCF_3CO_2$ in acetone for 6 h. It is worth noting that all the reactions took place with retention of the *fac*-C,C,C geometry of the chloride precursor, as assessed by NMR spectroscopy. This result is in contrast to the easy *fac*- to *mer*-isomerization that we found in the formation of the cyanide complex *mer*-$[Pt(pbt)_2(C_6F_5)(CN)]$ starting from the same precursor.[12a]

The complexes were isolated as white solids in moderate to high yields. They were fully characterised by IR spectroscopy, mass spectrometry, elemental analysis and multinuclear NMR spectroscopy (see the Experimental section and Fig. S1–S7† for details). The molecular structures were confirmed by X-ray diffraction for **1**, **4** and **6**. ESI(+) spectra showed a peak envelope compatible with cationic fragments of the formula $[Pt(pbt)_2(C_6F_5)(L)]^+$ for **1–6**, whereas the bimetallic complex **7** exhibited a peak for $[\{Pt(pbt)_2(C_6F_5)\}_2(bpyb) + PF_6]^+$.

The ^1H and $^{13}C\{^1H\}$ NMR spectra of all compounds showed two sets of resonances corresponding to the inequivalent pbt ligands due to the asymmetric nature of the coordination environment around the metal and signals due to the coordinated N-donor ligand (**1–5**, **7**). The most characteristic resonances in the proton spectra were the signals due to the *ortho* protons of the metalated C of the pbt groups, H^{11} and $H^{11'}$(pbt), which appeared as pseudo-triplets due to the additional space through dipolar coupling to the *o*-F of the C_6F_5 unit ($J_{H11-H10} \sim J_{H11-o\text{-}F} \sim$ 6–7 Hz), thus supporting the retention of the *fac*-C,C,C configuration. This spectroscopic feature was clearly visible for $H^{11'}$, which appeared in all compounds at a high field ($\delta \sim 6.88$). The coordination of the N-donor ligands was inferred by the low field shift of the *o*-H of the corresponding pyridine rings in relation to the free ligands (δ H^{14}: 9.10 **1** *vs.* 8.40, 4-Mepy; 9.10 **2** *vs.* 8.90, **pybt**; 9.06 **3** *vs.* 8.70, 4,4′-bipy; 8.90 **4** *vs.* 8.61, bpe; 9.02 **5**, **7** *vs.* 8.65 ppm, bpyb) and the presence of ^{195}Pt coupling ($^3J_{Pt-H} \sim$ 25 Hz). The $^{19}F\{^1H\}$ NMR spectra showed five signals corresponding to the C_6F_5 group with two *o*-F signals exhibiting Pt coupling constants ($^3J_{^{195}Pt-^{19}F}$ = 97–113.5 Hz), consistent with previously reported analogues,[12a,b] together with the expected doublet due to PF_6^- (δ −72.6) in complexes **1–5** and **7**. The coordination of $CF_3CO_2^-$ to the platinum in complex **6** was supported by the presence of platinum satellites in the resonance due to CF_3 (δ = −75.3, $^4J_{Pt-F}$ = 4.1 Hz). As noted before, the ^1H NMR spectrum of *fac*-$[Pt(pbt)_2(C_6F_5)(bpe)](PF_6)$ **4** revealed the presence of two isomers in a *ca.* 1 : 0.1 molar ratio, which were attributed to the two conformations *E* and *Z* of the 1,2-bis(4-pyridyl)ethylene (bpe) ligand. The major component is tentatively assigned to the *E*-form around the C=C double bond because this isomer is expected to reduce the steric constraint about the Pt centre. Unfortunately, the olefin protons overlapped with other resonances. The presence of the *Z* form, in a small amount, suggested that the bpe ligand suffers from easy photoisomerization. This light isomerization has been recently observed in bimetallic Pt^{II} compounds with the bpe bridging unit.[36] Indeed, control of the photoisomerization process in an acetone-d^6 solution, with a 125 W lamp, revealed that a final photostationary state between both isomers, with a proportion of 1 : 1.15 (*E* : *Z*), was reached after 40 min (Fig. S8†). It is worth noting that the *E* or *Z* orientation of the ligand caused a negligible influence on the chemical shifts of the fluorine resonances of C_6F_5, as assessed by $^{19}F\{^1H\}$ NMR spectroscopy.

X-ray crystallography

Crystals of complexes **1**, **4** and **6** were obtained by slow diffusion of *n*-hexane into a solution of the complexes in acetone at room temperature. The crystal structures of **1**·CH_3COCH_3, **4**·$2CH_3COCH_3$ and **6** are shown in Fig. 1. For complex **4**, two sets of conditions were used, in the dark and in the presence of ambient light. For crystals in the dark the quality of data collection, although not good enough, allowed us to confirm that the main complex formed has the *trans* (*E*) configuration at the olefinic double bond (Fig. 1b). For this complex, the crystals grown under ambient light were not of good quality either.

However, although the structure could not be completely refined, the connectivity of the structure was established and revealed a positional disorder of the bpe ligand in two positions, *E* and *Z* in a proportion of 60 and 40%, respectively (Fig. S9†). This result is consistent with the NMR studies and with previous work reported by Wang, *et al.* for triarylboron-functionalized Pt^{II} dinuclear complexes with bpe bridging unit, where the growth of the crystals, either at room or at low temperature, in the dark gave only the *E* isomer, whereas the

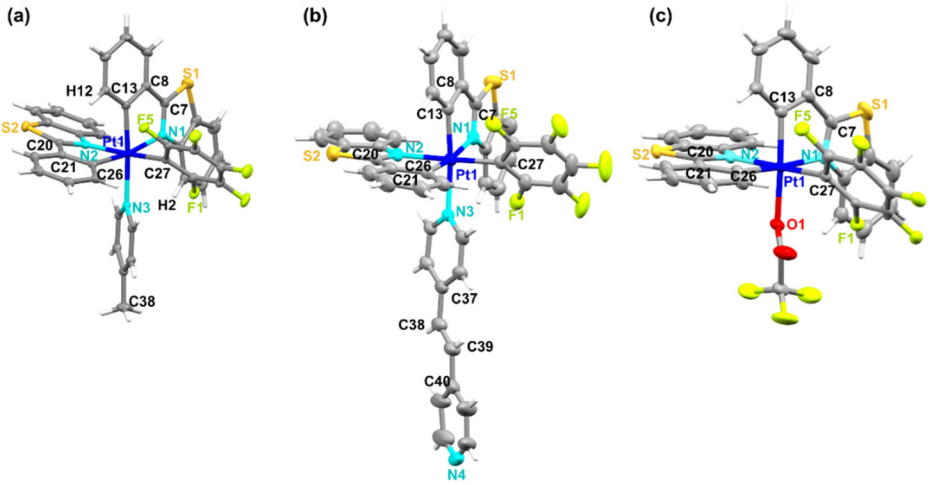

Fig. 1 Molecular view of the cations in (a) **1**·CH_3COCH_3, (b) [Pt(pbt)$_2$(C_6F_5)(*E*-bpe)](PF_6)·2CH_3COCH_3 (**4**·2CH_3COCH_3) (crystals grown in the dark) and (c) of **6**.

ambient light illumination was the key factor for *Z*-isomer formation.[36] The collected crystal data, refinement parameters, and selected bond lengths and angles are summarised in Tables S1 and S2.† The complexes were chiral, but crystalized in centrosymmetric space groups, with the two enantiomers (Δ and Λ) present in the unit cell (Δ enantiomer is depicted). The structures showed an octahedral geometry around the Pt center and confirmed the relative *fac* disposition of the three carbon atoms (*fac*-C,C,C). The Pt–N(2) bond distances *trans* to the metalated C_{pbt} [2.121(5)–2.135(5) Å] were shorter than those of Pt–N(1) [2.165(5)–2.301(6) Å], indicating a higher *trans* influence of C_{pbt} relative to $C_{C_6F_5}$. The Pt–N(3) lengths in complexes **1** [2.170(3) Å] and **4** [2.172(6) Å] were almost identical and within the range expected for these bonds. The Pt–C(13) distances in **1** and **4** [2.041(4) **1**, 2.042(7) Å **4**] were identical within the experimental error, according to a similar *trans* influence for the 4-Mepy and bpe ligands, whereas in complex **6** this distance [2.011(7) Å] was relatively shorter, in agreement with a lower *trans* influence of the trifluoroacetate ligand (O-donor). As far as we know, examples of X-ray structures of cyclometalated Pt^{IV} complexes with monodentate pyridines are very scarce.[37] In **4**, the bpe ligand adopted a *trans* configuration with a C38–C39 distance [1.321(10) Å] typical of a double bond, and it was essentially coplanar. The dihedral angle between the pyridine rings (given by the dihedral angle C37–C38–C39–C40) was 6.83°. Molecular packing revealed the presence of dimers generated by short $\pi_{pbt}\cdots\pi_{pbt}$ (~3.4–3.5 Å) interactions in complexes **1** and **4**, which further involved through $F_{C_6F_5}\cdots F_{C_6F_5}$ contacts (2.825 Å) in complex **1** (Fig. S10 and S11†). For **6**, only secondary contacts $F_{C_6F_5}\cdots\pi_{pbt}$ (2.927 Å), C–H···O (2.686 Å) and C–F···F_{CF_3} (2.764 Å) were observed (Fig. S12†).

Photophysical properties and theoretical calculations

Absorption spectra. The UV/VIS absorption spectra of all the complexes, recorded in dichloromethane solution at room temperature, are shown in Fig. 2 with the corresponding data summarized in Table S3.† The absorption spectra were very similar in the high energy region (λ < 300 nm) with absorptions mainly ascribed to ligand-based (pbt and L) transitions, although contributions from ligand to ligand (pbt, C_6F_5 to L) and ligand to metal (pbt to Pt) cannot be discarded. The low energy structured profiles for cations **1**, **3**, **5** and **6** were rather similar (ε = 12 000–22 000 mol^{-1} L cm^{-1}) and with minor changes in their maxima. A stronger and broader low energy feature was shown for the **pybt** complex (**2**, ε = 36 000) and the bimetallic derivative (**7**, ε = 28 000). In order to gain insight into the nature of low-lying absorptions, DFT/TD-DFT calculations were carried out for all complexes. Selected frontier orbitals and vertical excitation energies computed by TD-DFT/SCRF in CH_2Cl_2 with the orbital involved are provided in Fig. 3 and in the ESI (Fig. S13 and Tables S4–S6†).

For the cation $\mathbf{1}^+$ and for **6**, the frontier orbitals (H−3 to L+2) were located on the pbt groups with minor contribution

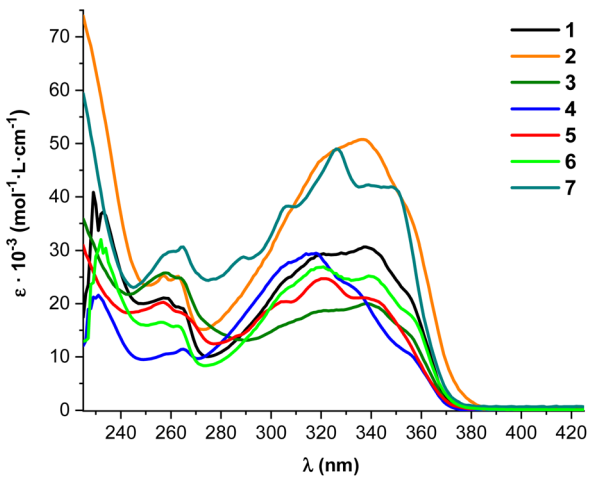

Fig. 2 Absorption spectra of complexes **1–7** in CH_2Cl_2 (5 × 10^{-5} M) at 298 K.

of the Pt and auxiliary ligands. In these complexes, the two most intense transitions (S_2 and S_3) have intraligand (IL) character located on the pbt groups, whereas S_1 with low oscillator strength (HOMO–LUMO transition) has mainly ligand to ligand charge transfer between non-equivalent pbt ligands (LLCT). In the cation $\mathbf{3}^+$, featuring the 4,4′-bpy ligand, the composition of the highest occupied orbitals and the LUMO is similar to those of $\mathbf{1}^+$ and **6** but L+1 and L+2, which have a notable contribution to 4,4′-bpy (L+1 69%; L+2 26%), are very close in energy. The more intense transition S_2 (339.6 nm) has IL nature but the close S_3 has mainly ligand to ligand charge transfer character (pbt to 4,4′-bpy). For the cations featuring 4-pyridylbenzothiazole (**pybt**) $\mathbf{2}^+$, 1,2-bis-(4-pyridyl)ethylene (bpe) $\mathbf{4}^+$ and 1,4-bis-(pyridyl)butadiyne (bpyb) $\mathbf{5}^+$, the corresponding LUMO is essentially located on the N-donor ligand **pybt**, bpe and bpyb (L′), respectively, whereas the cyclometalated pbt ligands contribute to L+1 and L+2. The HOMOs are located on the pbt ligands and, the N-donor contributes to the closest H−1 and H−2 (see Fig. 3).

In $\mathbf{2}^+$ and $\mathbf{5}^+$ the calculated most intense transition (S_5 for $\mathbf{2}^+$, 343 nm; S_3 for $\mathbf{5}^+$, 367 nm) can be theoretically ascribed to ^{1}IL′CT (**pybt** $\mathbf{2}^+$; bpyb $\mathbf{5}^+$) with some ^{1}LL′CT (pbt to **pybt** $\mathbf{2}^+$ or

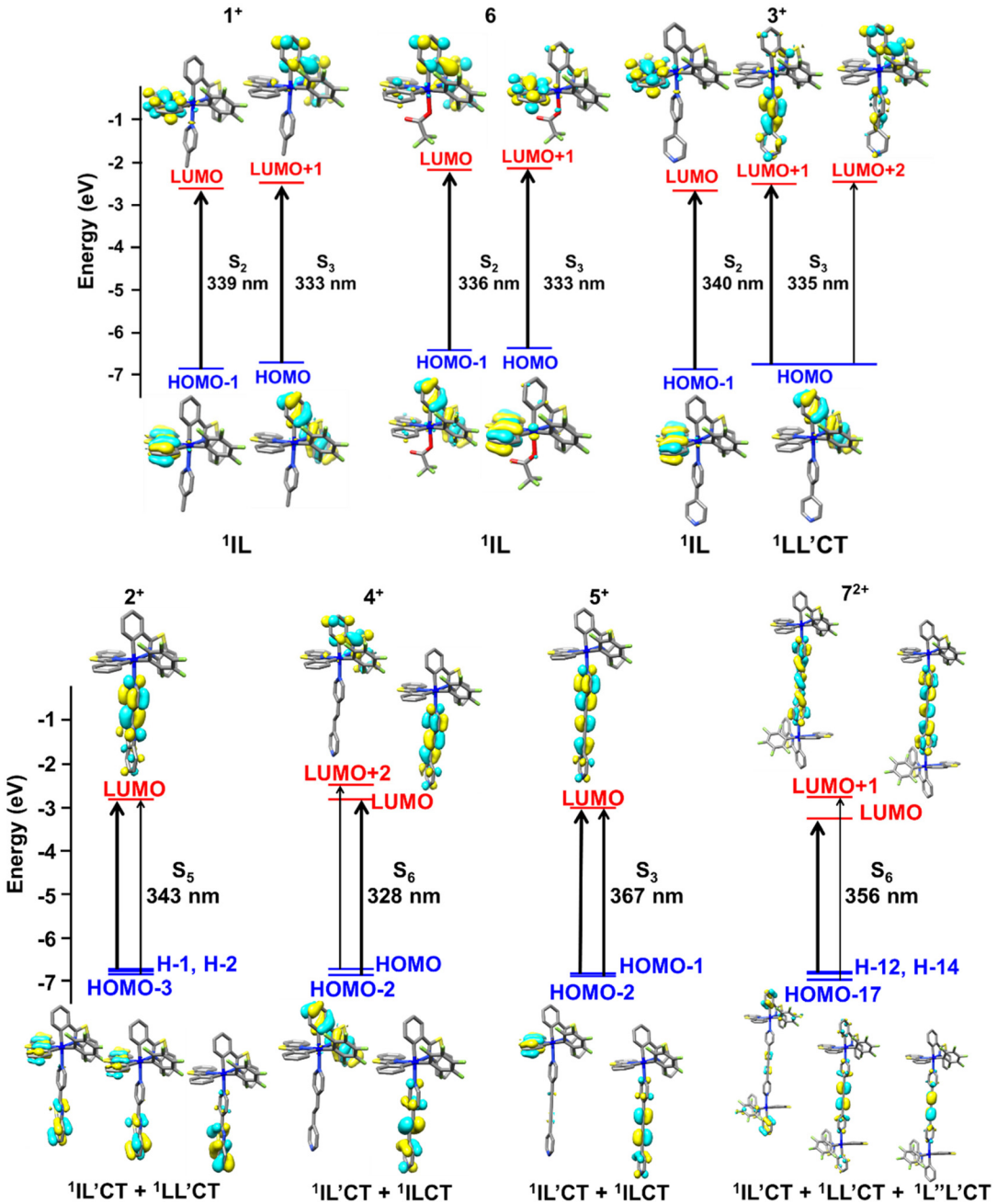

Fig. 3 Schematic representation of selected excitations for $\mathbf{1}^+$–$\mathbf{5}^+$, **6** and $\mathbf{7}^{2+}$.

bpyb 5^+) contribution, while in 4^+ S_6 (328 nm) has ^{1}IL′CT (bpe) with some ^{1}ILCT (pbt) character. In 2^+, S_4 (351 nm), with lower intensity, has ^{1}LLCT (pbt → pbt) character with minor ^{1}LL′CT/^{1}IL′CT contribution and in 4^+ the closest (less intense) transition, S_4 (339 nm), is located in the pbt ligands and S_5 (333 nm) has also a mixture of ^{1}IL′CT/^{1}ILCT characters. In the bimetallic complex cation, 7^{2+}, the LUMO (and L+1) is located in the bridging bpyb ligand, whereas the highest occupied orbitals (H−3 to HOMO) are located on the cyclometalated pbt. For this complex, the most intense transition (S_6 calc. 356 nm) with a complex configuration [H−14 (54%); H−12 (11%) → LUMO; H−17 → L+1 (15%)] is ascribed to an ^{1}IL′CT (L′ = bpyb) with minor ligand to ligand charge transfer contribution (pbt, C_6F_5 to bpyb).

Complex **4** absorbs light, as already mentioned, which results in its isomerization. Thus, a CH_2Cl_2 solution (5×10^{-5} M) of crystals of the bpe complex (mixture of 90 : 10, *E* : *Z* forms) was irradiated using a monochromator centered at 320 nm during 1 h (Fig. 4). The irradiation process, monitored by UV-VIS spectroscopy, displays a decreased low energy band centred at ∼315 nm and an increased high energy band at ∼265 nm, reaching the photostationary state after 15 minutes of irradiation (Fig. 4a). We tentatively assign this change in the absorption spectra to an isomerization process of the C=C bond in the bpe ligand from the *E*-isomer to the *Z*-form (Fig. 4b). Once the photostationary state was reached, subsequent irradiation at 255 nm with a hand-UV lamp was performed to explore if the process could be reversible but, unfortunately, no changes in the absorption of the mixture were observed under these conditions.

Emission spectra. The photoluminescent properties were examined in CH_2Cl_2 solution (298 and 77 K), in the solid state (298 and 77 K) and in a polystyrene film (PS) with a doping concentration of 10% at 298 K. Selected emission spectra are shown in Fig. 5–8, overlaid excitation and absorption spectra are shown in Fig. 5 and S14† and the photophysical data are summarized in Table 1. Complex **4** is only emissive in glassy solution at 77 K. In this complex, we attribute the quenching of the emission at room temperature, upon photoexcitation, to the occurrence of an enhanced intramolecular *E* to *Z* isomerization process of the 1,2-bis-(4-pyridyl)ethylene ligand. This assumption is also supported by theoretical calculations (in CH_2Cl_2 solution and in the gas phase).

In this complex, T_1 originates mainly from H−2 to the LUMO, which are located on the bpe ligand. The spin density of the optimized T_1 reveals that in the excited state the ligand adopts a *cis* or *Z* configuration (Fig. 5). In the optimized T_1, the olefinic C38–C39 distance increases to 1.466 Å and the dihedral C37–C38–C39–C40 angle decreases to 93.36°, relative to the values of 1.349 Å and 179.66° in the ground state S_0 (Table S4†). The process seems to be efficient at 298 K and somewhat reduced in the frozen matrix. Thus, in glassy CH_2Cl_2 solution at 77 K, the complex exhibits two overlapping structured bands with emission maxima starting at 495 (λ_{exc} 340–350 nm) and 515 nm (λ_{exc} 380–400 nm), respectively. As seen in Fig. 5, both bands are related to two distinct excitation spectra, partially overlapping the absorption profile, suggesting the presence of the two isomers, although some degree of aggregation cannot be excluded. The emission bands are tentatively attributed to T_2 and T_3 intraligand transitions located on the coordinated pbt ligands (^{3}ILCT) of both isomers (*E* and *Z*).

Complex **2**, featuring the 4-pyridylbenzothiazole ligand, shows a dual emission in CH_2Cl_2 and in the PS film at 298 K formed by a low energy structured feature (491, 530, 575, and 627 nm, CH_2Cl_2) together with an unstructured band centred at 420 nm. For comparison, the emission of the **pybt** ligand was also recorded. The ligand exhibits an intense fluorescence band at 385 nm and a small structured phosphorescence feature at 530 nm (CH_2Cl_2, λ_{exc} 330 nm Fig. S15a†). As expected, for this complex, the low energy emission is quenched in an aerated solution, being therefore associated with phosphorescence, whereas the one at higher energy is essentially unaffected under these conditions (Fig. 6). The insensitivity against oxygen, the short lifetime and its similarity to the fluorescence from **pybt** allowed us to ascribe the high-energy emission band to $^1\pi\pi^*$ located on the **pybt** ligand. Excitation spectra monitored at the maximum of either band coincide with the electronic absorption spectrum, ruling out the possibility that any of the bands originate from impurities.

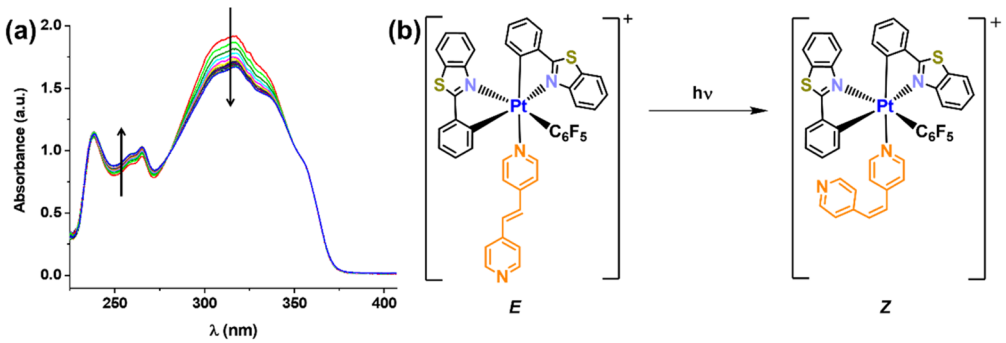

Fig. 4 (a) Change in the absorption spectra of **4** (crystals, 90 : 10, *E* : *Z*) in CH_2Cl_2 (5×10^{-5} M) with 320 nm irradiation; (b) photoisomerization of complex **4**.

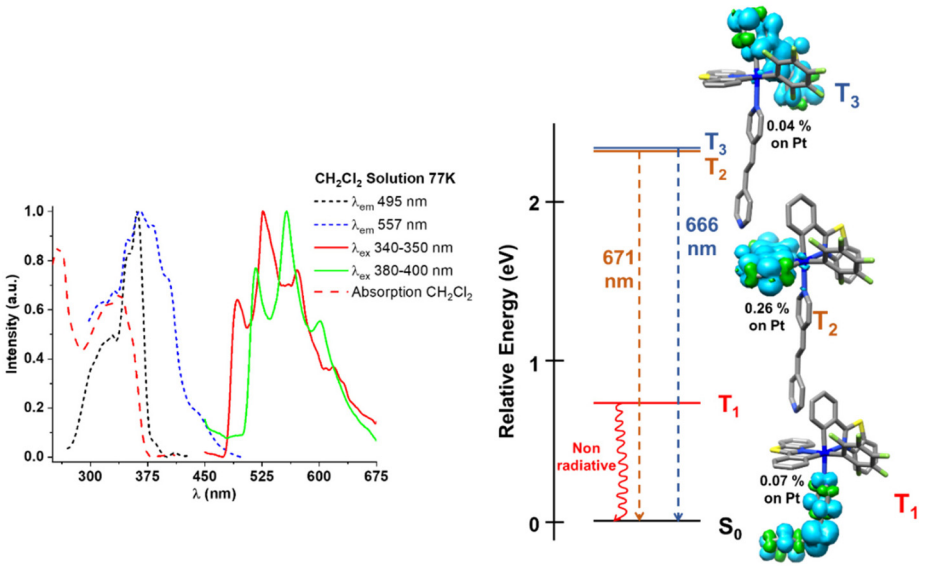

Fig. 5 Overlaid excitation, absorption (CH_2Cl_2, 298 K) and emission spectra of **4** in glassy CH_2Cl_2 solution (5×10^{-5} M) at 77 K and the spin density distribution of the optimized T_1–T_3 triplet states in the gas phase for cation $\mathbf{4}^+$.

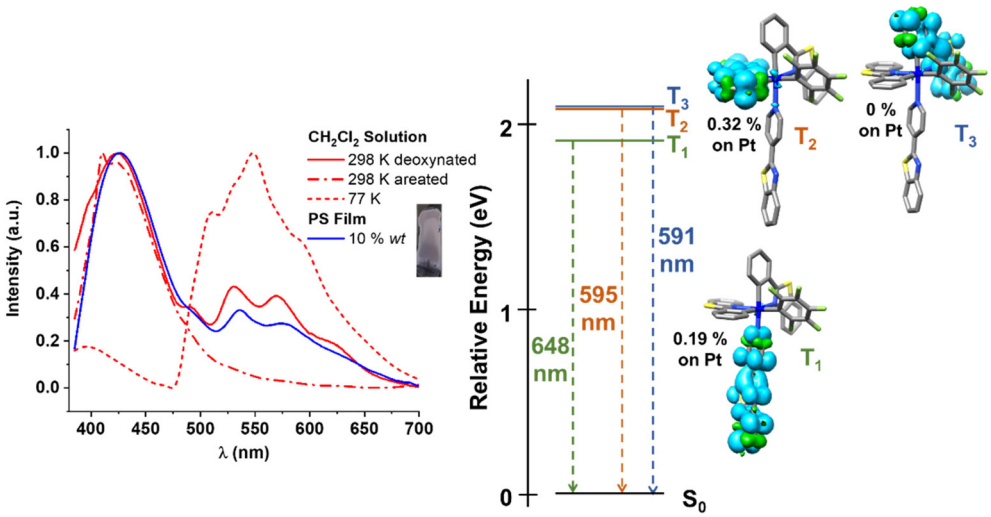

Fig. 6 Emission spectra (λ_{ex} 365 nm) in several media (deoxygenated and aerated CH_2Cl_2 solution, glassy and PS 10% w/w) of **2** and the spin density distribution of the optimized T_1–T_3 triplet states in CH_2Cl_2 for $\mathbf{2}^+$.

In glassy CH_2Cl_2 solution (77 K), only the broad structured low energy emission, slightly red shifted (λ_{em} 511 nm), is observed. The SOMO and SOMO−1 and the spin density surface for the optimized T_1 of $\mathbf{2}^+$ are located on the **pybt** ligand, suggesting that the low energy emission has mainly ^{3}IL′ character (Fig. 6 and Table S7†). However, we note that the measured decays on the first two peaks (~490 and 530 nm) fit to two components, suggestive of a mixture of close emissive states and calculations indicate that T_2 and T_3, of ^{3}ILCT character, are relatively close in energy.

Complexes **1**, **3**, and **5**–**7** display in fluid solution and in a polystyrene film at 298 K a long-lived structured emission band with a minor change in their λ_{em} maxima (492–504 nm) (Fig. 7 and 8). Upon cooling the solutions at 77 K, the emission of complexes **1**, **3** and **6** is slightly blue shifted and the lifetime, which fits to two components, increases notably (see Table 1). According to calculations, for $\mathbf{1}^+$, $\mathbf{3}^+$ and **6** the SOMO and SOMO–1 are located on one of the cyclometalated pbt ligands (Table S7†). In these complexes, the T_1 and T_2 optimized triplets are very close in energy and their spin density surfaces are located on the pbt ligands, indicating that the emission has ^{3}ILCT character. In $\mathbf{1}^+$ and **6**, T_1 is located on the $pbt_{(1)}$ *trans* to C_6F_5 and T_2 is located on the $pbt_{(2)}$ *trans* to 4-Mepy in $\mathbf{1}^+$ or *trans* to $OCOCF_3$ in **6**, whereas in $\mathbf{3}^+$ both

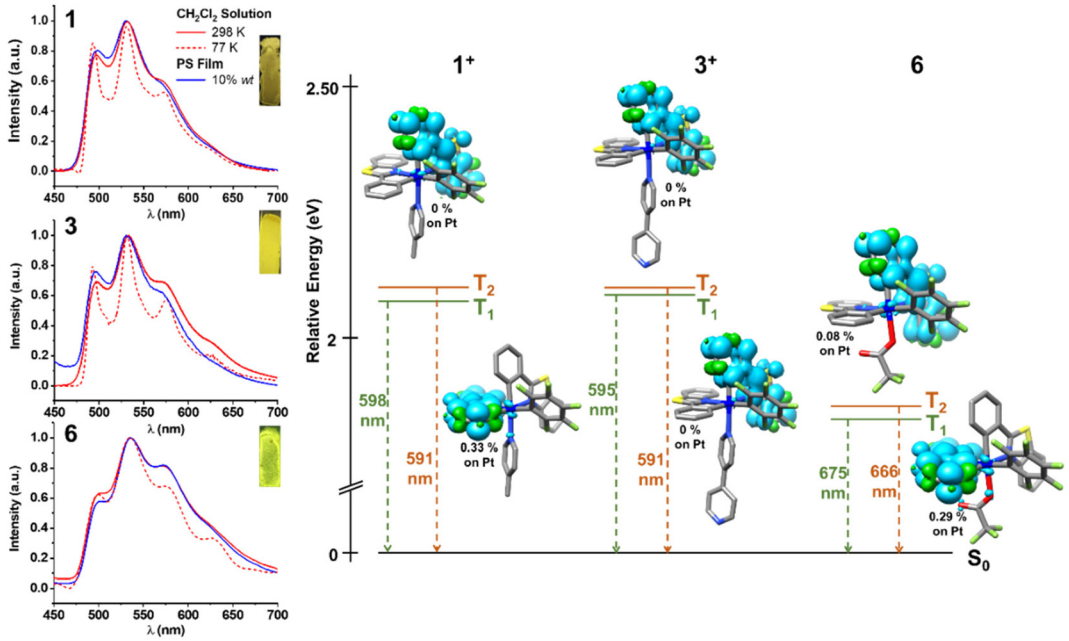

Fig. 7 Emission spectra (λ_{ex} 365 nm) of $\mathbf{1}^{+}$, $\mathbf{3}^{+}$ and **6** in several media and the spin density distribution of the optimized T_1–T_2 triplet states in CH_2Cl_2.

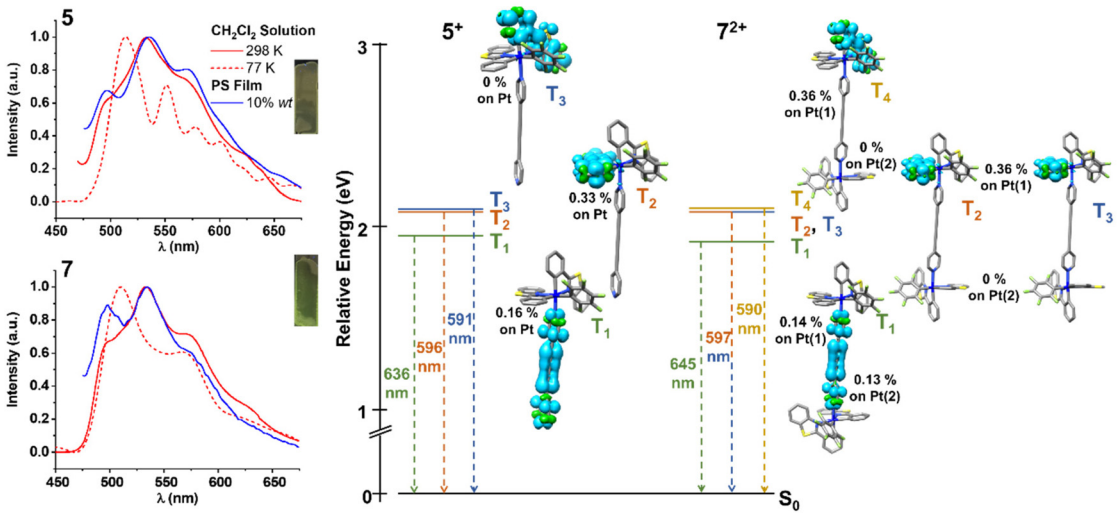

Fig. 8 Emission spectra (λ_{ex} 365 nm) of **5** and **7** in several media and the spin density distribution of the optimized T_n triplet states for the cations in CH_2Cl_2.

triplets are located on the $pbt_{(2)}$ *trans* to 4,4′-bpy. For **5** and **7** featuring the bpyb ligand (Fig. 8), the emission profiles in fluid solution and in the PS film at 298 K are similar, exhibiting a broad structured emission with $\lambda_{max} \sim 495$ nm for **5** and the emission slightly red shifted for **7** (498 nm). For both complexes, the spin density of the optimized T_1 in the cations is located on the low-lying 1,4-bis-(pyridyl)butadiyne ligand, but T_2 and T_3 (and also T_4 in $\mathbf{7}^{2+}$), of ^{3}ILCT (pbt) character, are close in energy (Fig. 8). As noted in Table 1, the lifetimes fit to several components (two for **5** and even three for **7** in PS), indicating that the emission consists of different transitions with different energies and radiative rates. The emission is therefore ascribed to a mixture of close ^{3}IL′/^{3}ILCT excited states. In glassy solution, the emission profile of **5** is vibronically more complex and red-shifted to 514 nm, close to the phosphorescence of free bpyb (525 nm, Fig. S15†), indicating more contribution from the low-lying T_1 located on the bpyb unit.

The measured phosphorescence quantum yields in solution of this series of Pt^{IV} complexes are relatively low, in the range of 0.8–1.2%, and they increase in the rigid PS film by 1.6 to

Table 1 Photophysical data for complexes **1–7**[a]

	CH_2Cl_2[b]			PS[c]		$\phi(^1O_2)$[d]/%
	298 K		77 K	298 K		Aerated MeCN
	λ_{max}[e]/nm [τ/μs]	ϕ/%	λ_{max}[e]/nm [τ/μs]	λ_{max}[e]/nm [τ/μs]	ϕ/%	
1	496 [2.9]	1.2	493 [227.3, 82%; 73.4, 18%]	499 [2.9]	4.9	66
2	420 [0.3], 491 [2.5], 530 [2.7, 36%; 0.9, 64%] 575, 627_{sh}	1.0	511 [11.9, 61%; 264.3, 39%]	422 [2.5, 42%; 11.8, 58%], 491 [13.3, 90%; 49.7, 10%], 535 [11.9, 82%; 49.9, 18%]	1.2	74
3	493 [3.5]	1.0	493 [219.5, 81%; 18.8, 19%]	497 [2.2]	3.2	86
4	[f]	[f]	495[g] [197.2, 75%; 21.5, 25%]; 515[h] [178, 70%; 26.3; 30%]	[f]	[f]	
5	495 [0.5, 21%; 3.2, 79%]	0.8	514 [305.5, 59%; 22.6, 41%]	495 [0.8, 90%; 34.7, 10%]	1.3	
6	504 [3.6, 39%; 11.2, 61%]	1.2	500 [150.8, 74%; 21.6, 26%]	502 [24.0, 84%; 57.7, 16%]	5.5	82
7	498 [2.1]	0.6	511 [1200.5, 50%; 102.2, 50%]	498 [3.11, 61%; 25.0, 28%, 68.6, 11%]	1.5	

[a] λ_{ex} 365 nm. [b] Deoxygenated, 5×10^{-5} M. [c] 10 wt%. [d] λ_{ex} = 365 nm. [e] Highest energy peaks of the phosphorescence band. [f] Non-emissive. [g] λ_{ex} = 340–350 nm. [h] λ_{ex} = 380–400 nm.

4.6-fold. This is attributed to the suppression of molecular vibrations and the oxygen exclusion by the film. In the solid state, only complexes **1** and **6** are emissive, exhibiting red shifted weak emissions (Fig. S16†). The notable quenching in the solid state can be attributed to the low energy trap states originated from strong intermolecular aggregation through non-covalent interactions.[38]

Singlet oxygen measurements. We examined the ability of complexes **1**, **2**, **3** and **6** to generate $^1O_2$. Singlet oxygen is considered as the main cytotoxic species in photodynamic therapy through a type II (energy transfer) mechanism. The triplet energy level (T_1) is a critical parameter for efficient energy transfer (ET) to $^3O_2$ in the generation of $^1O_2$. Indeed, the triplet energy level of an efficient $^1O_2$ photosensitizer has to be higher than the energy necessary to allow an efficient energy transfer to ground state molecular oxygen ($^3O_2$ 0.98 eV) and promote the formation of $^1O_2$.[39] The triplet state is of appropriate energy for all complexes (range 1.86–2.08 eV) and the singlet oxygen sensitization was measured by emission spectroscopy. The efficiency of $^1O_2$ generation at 298 K in an aerated acetonitrile solution (5×10^{-5} M) was directly determined by monitoring the emission band at 1276 nm using a near-infrared detector upon excitation at 365 nm (see Fig. 9 for **6**). As an universal standard to quantify this emission, phenalenone (PN) can be used.[40] Thus, the singlet oxygen quantum yields have been calculated (see ESI†) in comparison with free PN in an aerated acetonitrile as a reference (QY of 100%).[40b] The high values of $\phi(^1O_2)$ obtained, ranging from 66 to 86% (Table 1), suggest that these complexes are efficient photosensitizers.

Biological studies

Stability assays. First, the stability of complexes **1–3** and **6** was evaluated by ^{1}H NMR in DMSO-d^6 solution and DMSO-d^6/D_2O (9/1) (Fig. S17–S20†) or UV-Vis spectroscopy in DMSO-cellular medium (Fig. S21†). ^{1}H NMR stability studies showed that complexes **1** and **3** are stable in DMSO or DMSO/D_2O (9/1) after 72 h (Fig. S17 and S19†). However, complex **2** suffers a ligand exchange process involving the displacement of **pybt** by a DMSO molecule, as is evident by ^{1}H NMR (Fig. S18†) and especially in the UV-Vis where appears after 6 h a band at 290 nm, corresponding to the free **pybt** ligand (Fig. S21†). However, all attempts we made to prepare the expected cationic $[Pt(pbt)_2(C_6F_5)(DMSO)](PF_6)$ complex were unsuccessful. In the case of complex **6**, the evolution is somewhat more complex, appearing in DMSO/D_2O (9/1) at least three different species, likely by displacement of the trifluoroacetate ligand, as it is supported by the presence of three *para*-fluorine signals in the $^{19}F\{^1H\}$ NMR spectra due to C_6F_5 groups (Fig. S20†). The photostability of **6** was also assessed by ^{1}H NMR (see below and Fig. S22 and S23†) and UV-vis spectroscopy (Fig. S24†).

On the other hand, since it is generally accepted that Pt^{IV} compounds are rapidly reduced under physiological conditions by cellular reducing agents,[26] the possible reaction of **1** with ascorbic acid (1 : 10 molar ratio) in DMSO-d^6/D_2O (9/1)

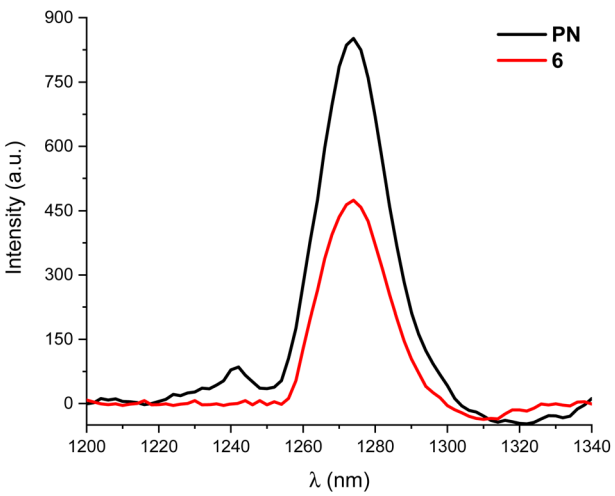

Fig. 9 Emission band of singlet oxygen from fresh solution of **6** in MeCN in comparison with that of phenalenone (PN) (λ_{ex} 365 nm).

was monitored by ^{1}H and $^{19}F\{^{1}H\}$ NMR spectroscopy (Fig. S25 and S26†) as a representative example. No evidence of the reaction was observed excluding easy reduction under biological conditions.

Cytotoxic activity and selectivity index. The IC_{50} values of complexes **1–3** and **6** and the **pybt** ligand were determined against two different cell lines, human tumour (A549 cells, lung carcinoma and HeLa cells, cervix carcinoma) and non-tumoral BEAS-2B (bronchial epithelium), after cellular exposure to the compounds for 72 h and compared to cisplatin as a reference (Table 2 and Fig. S27†). Complexes **1**, **2** and **3** were more cytotoxic than cisplatin in both A549 [IC_{50}: 1.09 (**1**); 0.32 (**2**); 0.66 (**3**) *vs.* 6.45 (cisplatin)] and HeLa [IC_{50}: 1.11 (**1**); 0.39 (**2**); 4.38 (**3**) *vs.* 13.60 (cisplatin)] cell lines (Table 2). As complex **2** suffers exchange of the **pybt** ligand for DMSO, the cytotoxicity values of the **pybt** ligand were also determined. The cytotoxicity of **pybt** was almost negligible towards A549 (IC_{50}: 99.59 μM) and BEAS-2B (IC_{50}: 133.90 μM) cell lines; however, it showed high toxicity against HeLa cells (IC_{50}: 8.96 μM). In this sense, it was previously reported that **pybt** also shows high cytotoxicity towards breast cancer cell lines (IC_{50} between 1 and 10 μM).[41] These results indicate that the cytotoxicity of **pybt** is selective for certain cell lines. Therefore, the occurrence of some synergic effect with the liberated free ligand in the measured activity of complex **2** towards HeLa cells is possible. The neutral complex **6**, which contains a trifluoroacetate group, showed mild cytotoxic activity, (29.40 and 51.60 in A549 and HeLa cells, respectively) (Table 2 and Fig. S27†). IC_{50} values for complexes **1** and **2** were found to be similar in both tumour cell lines; however, complexes **3** and **6** were more active towards the A549 cell line rather than the HeLa cell line, in accordance with our previous results.[43]

Furthermore, to evaluate the selectivity (SI) of these complexes towards tumour cell lines, we had tested the cytotoxic activity against a normal epithelial lung virus-transformed (BEAS-2B) non-tumour cell line. Cisplatin showed an IC_{50} value towards BEAS-2B of 1.74 μM, slightly lower than those for A549 and HeLa cells, therefore rendering low selectivity of this anti-cancer drug for these cell lines (0.27 and 0.13, respectively)[28e] (Table 2), in good agreement with previously reported values.[44] Actually, compounds with a SI values of <2 are assumed to give general toxicity.[45] Based on the IC_{50} assessment, the better values of the selectivity index (SI) were given by the **pybt** ligand in HeLa cells (14.94) as well as complexes **1** and **2** in both tumoral A549 [3.17 (**1**); 4.75 (**2**)] and HeLa [3.11 (**1**); 3.83 (**2**)] cells, due to their higher cytotoxic activity in these cells compared to non-tumoral BEAS-2B cells, and to lower extent by complex **3** towards A549 cells (2.20) against non-tumour BEAS-2B cells. SI values for complex **6** were 1.71 (A549 cells) and 0.97 (HeLa cells), which indicated low selective toxicity towards cancer cells (Table 2). The lowest SI values (<1) were shown by complex **3** in HeLa cells (0.33). Low SI values (<2) for related platinum derivatives and other organometallic complexes with cytotoxic activities toward A549, HeLa, and other cancer cell lines have been previously described.[27a,42,46]

Photoinduced cytotoxicity. The capability of the complexes working as photosensitizers (PS) is well stablished in Ir^{III} and also in Pt^{II} complexes.[23,30b,47] Due to their ability to generate $^{1}O_2$ upon irradiation and their photostability, they can be considered as potential tools in phototheranostics.[35c,48] We decided to evaluate the potential use of complex **6** in photodynamic therapy based on its mild cytotoxic effects under normal cell culture conditions. First, complex **6** showed good photostability in DMSO-d^6 and DMSO-d^6/D_2O (9/1) (supported by ^{1}H and $^{19}F\{^{1}H\}$ NMR, Fig. S22 and S23†) and UV-VIS absorption in DMSO or DMSO-cellular medium (Fig. S24†) by exposure to similar conditions to that employed in the photoinduced activity assays. In order to assess its photobiological activity, A549 cells were treated with complex **6** in Hank's balanced salt solution (HBSS) for 1 h at 37 °C to allow cellular interaction and internalization. Then, A549 cells were irradiated with a 396 nm LED lamp located 91 mm apart (5 mW cm^{-2}) for 15 minutes (see the ESI†). After irradiation, the cells were washed and incubated in complete RPMI medium (without complex **6**) for another 72 hours. Finally, cell viability (IC_{50}) was assessed by MTS test, as described in the ESI.† As shown in Fig. 10, UV light irradiation during 15 minutes enhanced the antitumor activity, leading to an IC_{50} value of 5.75 μM, in relation to their basal non-UV-irradiated cell survival rates (50.20 μM). UV irradiation caused 10% mortality in

Table 2 Cytotoxicity IC_{50} values[a] (μM) and selectivity index[b] of complexes **1**, **2**, **3** and **6** in A549, HeLa and BEAS-2B human cell lines compared with those of cisplatin

	IC_{50}[a]			SI[b]	
Complex	A549	HeLa	BEAS-2B	A549	HeLa
1	1.09 ± 0.02	1.11 ± 0.12	3.45 ± 0.51	3.17	3.11
2	0.32 ± 0.12	0.39 ± 0.07	1.51 ± 0.10	4.75	3.83
3	0.66 ± 0.15	4.38 ± 0.50	1.45 ± 0.29	2.20	0.33
6	29.40 ± 4.81	51.60 ± 7.97	50.29 ± 4.23	1.71	0.97
pybt	99.59 ± 8.55	8.96 ± 0.36	133.90 ± 2.50	1.34	14.94
Cisplatin	6.45 ± 0.47[c]	13.60 ± 0.99[d]	1.74 ± 0.16[e]	0.27	0.13

[a] IC_{50} values are presented as the mean ± standard error of the mean of three different experiments. [b] Selectivity index (SI) = IC_{50} of non-tumor cells (BEAS-2B)/IC_{50} cancer cells (A549 or HeLa), as described in ref. 42. [c] As determined in ref. 35b. [d] As determined in ref. 35a. [e] As determined in ref. 28e.

A549 cells without the complex compared to non-irradiated cells. This value was subtracted at all points of the cell survival curve in order to obtain the IC_{50} value of photoinduced cytotoxicity (Fig. 10).

Relative lipophilicity. To correlate cytotoxic activity and lipophilicity, the relative hydrophobicity of the selected complexes **1–3** and **6** was measured by RP-UPLC. All compounds were dissolved in acetonitrile (~1 ppm) and the mobile phase used was a mixture of A (acetonitrile with 0.1% HCOOH) and B (H_2O with 0.1% HCOOH). The hydrophilic behavior was based on the retention times (t_R) that account for the interaction and/or the affinity of the complex for the hydrophobic stationary phase (Acquity UPCL BEH C18) or the hydrophilic mobile phase. Complexes with more lipophilicity should have longer t_R.[35c,49] The neutral complex **6** shows higher retention time than the cationic derivatives (complex/t_R min: **1**/3.8; **2**/4.9; **3**/3.0 *vs.* **6**/7.2). Complex **3** exhibits two different retention peaks, presumably due to the generation of some amount of a dinuclear platinum complex $\{[Pt(pbt)_2(C_6F_5)]_2(\mu\text{-}4,4'\text{-bpy})\}(PF_6)_2$. RP-UPLC was coupled with a QTOF mass spectrometer ESI(+) (Fig. S28,† upper panel). All complexes show, in their retention time, a similar pattern with the molecular peak $[M]^+$ for the cationic complexes **1–3** (*m*/*z* 875 **1**, 994 **2**, 939 **3**), $[M + Na]^+$ for **6** (*m*/*z* 917) and for all of them, the peak corresponding to the loss of the N-donor ligand (for **1–3**) or the $OCOCF_3$ group (for **6**) (*m*/*z* 782 $[M - L]^+$) (Fig. S28,† lower panel). Curiously, the most lipophilic complex **6** demonstrated a relatively low cytotoxicity, a fact that could be attributed to its neutral nature. As seen in Table 2, we only can establish a relationship between the lipophilicity and cytotoxic activity for the cationic complexes in HeLa cells, in which the highest cytotoxicity was found for the most lipophilic complex **2** [(t_R)/IC_{50}: 4.9/0.39 (**2**); 3.8/1.11 (**1**); 3/4.38 (**3**)].

Interaction of complexes with DNA. Knowing their cytotoxic activity, the interaction of Pt^{IV} **1–3** and **6** complexes with DNA was studied by their ability to modify the electrophoretic mobility of the supercoiled covalently closed circular (CCC) and the open circular (OC) forms of pBR322 plasmid DNA (Fig. S29†). To provide a basis for comparison, the incubation of DNA with cisplatin and the **pybt** ligand was also performed at the same concentrations and under the same conditions. The binding of cisplatin to plasmid DNA, for instance, results in a decrease in the mobility of the CCC form and an increase in the mobility of the OC form (Fig. S29,† left panel).[42,50] No electrophoretic mobility changes were observed after DNA treatment with any of the complexes tested (**1–3**, **6** and **pybt**) (Fig. S29† and data not shown), thus indicating that these compounds were either not reacting with the DNA or not altering the DNA mobility in agarose gels.

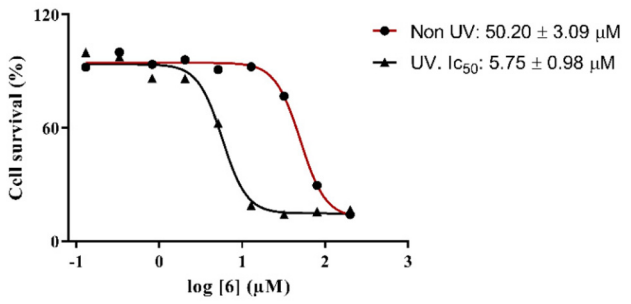

Fig. 10 Dose–response curves of the A549 cell line treated with complex **6** either with (triangles) or without (circles) UV light: irradiation with a UV 396 nm LED for 15 min, followed by MTS cytotoxic assay performed after 72 h. Non-UV and non-irradiated cells were manipulated identically to UV-irradiated ones. IC_{50} values are presented as the mean ± standard error of the mean of three different experiments performed in sextuplicate.

Conclusions

A series of mononuclear luminescent Pt^{IV} derivatives, *fac*-$[Pt(pbt)_2(C_6F_5)L]^{n+}$ (*n* = 1, 0, **1–6**), and a dinuclear complex $[\{Pt(pbt)_2(C_6F_5)\}_2(\mu\text{-bpyb})](PF_6)_2$ **7** have been synthesized and characterized and their optical properties were examined in detail. Complexes **1** (L = 4-Mepy), **3** (L = 4,4′-bpy) and **6** ($^-OCOCF_3$) exhibit typical ^{3}ILCT phosphorescence located on the cyclometalated pbt ligand. However, the incorporation of auxiliary ligands with stronger delocalization induces its participation in the low-lying emitting states. Thus, **5** (bpyb) and **7** display emissions ascribed to a mixture of close ^{3}IL′(N donor)/^{3}ILCT(pbt) excited states and **2** (L = **pybt**) shows both fluorescence and phosphorescence at 298 K, located on the low lying **pybt**. Complex **4** (L = bpe) was isolated as an *E*/*Z* mixture of 90/10 that photoisomerizes to a steady state of *E*/*Z* (~46/54). The quenching of the emission for **4** at room temperature is attributed to an easy intramolecular *E*/*Z* isomerization of the bpe ligand in the T_1 state and the two closely overlapping emission bands observed in glassy solution at 77 K are attributed to close (T_2 and T_3) intraligand transitions ^{3}ILCT (pbt) in both isomers. Complexes **1–3** and **6** showed remarkable singlet oxygen generation in aerated solution and was directly measured with the singlet oxygen emission at 1276 nm. The high $\phi(^1O_2)$ (66–86%) suggests that these complexes are efficient photosensitizers.

Cationic complexes **1–3** exhibited, under the usual experimental conditions, IC_{50} values in the low nanomolar range towards A549 and HeLa tumour cell lines, resulting in markedly more cytotoxicity than against the non-tumoral BEAS-2B cells (except complex **3** in HeLa cells). The neutral complex **6** was the least cytotoxic, but under photoirradiation (15 min) it exhibited high antiproliferative activity against the A549 cell line. These complexes are rare examples of anticancer luminescent cyclometalated Pt^{IV} complexes. The relative lipophilicities, according to RP-UPLC-QTOF-MS, followed the sequence of **3** < **1** < **2** < **6**. Only for cationic complexes these results can be related to the cytotoxicity in HeLa cells, being the more lipophilic and more cytotoxic against HeLa cell lines. The binding experiments with the pBR322 plasmid DNA revealed that complexes **1–3** and **6** do not alter the cell cycle progression, which indicated that they do not target nuclear DNA and exert their

anticancer activity through mechanisms that are different from that of cisplatin.

Conflicts of interest

There are no conflicts to declare.

Acknowledgements

This work was supported by the Spanish Ministerio de Ciencia e Innovación (project PID2019-109742GB-I00) funded by MCIN/AIE/10.13039/501100011033, the "ERDF A way of making Europe" and the "European Union" and by the ADER (Gobiernode La Rioja; Project 2017-I-IDD-00031). D. G. S. is grateful to UR for a PhD grant.

References

1 (*a*) A. Gualandi, F. Calogero, A. Martinelli, A. Quintavalla, M. Marchini, P. Ceroni, M. Lombardo and P. G. Cozzi, *Dalton Trans.*, 2020, **49**, 14497–14505; (*b*) Y. Wang, C. Zheng, M. Liu, W. Wei, J. Gao, Y. Zhang and P. Deng, *Chem. Commun.*, 2021, **57**, 3857–3860.

2 P.-Y. Ho, C.-L. Ho and W.-Y. Wong, *Coord. Chem. Rev.*, 2020, **413**, 213267.

3 (*a*) R. Guan, L. Xie, L. Ji and H. Chao, *Eur. J. Inorg. Chem.*, 2020, 3978–3986; (*b*) G.-X. Xu, L. C.-C. Lee, C. W.-C. Kwok, P. K.-K. Leung, J.-H. Zhu and K. K.-W. Lo, *Eur. J. Inorg. Chem.*, 2021, 3432–3442; (*c*) B. F. Hohlfeld, B. Gitter, C. J. Kingsbury, K. J. Flanagan, D. Steen, G. D. Wieland, N. Kulak, M. O. Senge and A. Wiehe, *Chem. – Eur. J.*, 2021, **27**, 6440–6459.

4 (*a*) B. Pashaei, S. Karimi, H. Shahroosvand, P. Abbasi, M. Pilkington, A. Bartolotta, E. Fresta, J. Fernandez-Cestau, R. D. Costa and F. Bonaccorso, *Chem. Soc. Rev.*, 2019, **48**, 5033–5139; (*b*) X. Zhang, Y. Hou, X. Xiao, X. Chen, M. Hu, X. Geng, Z. Wang and J. Zhao, *Coord. Chem. Rev.*, 2020, **417**, 213371; (*c*) S. Lee and W.-S. Han, *Inorg. Chem. Front.*, 2020, **7**, 2396–2422.

5 (*a*) M. L. Buil, M. A. Esteruelas and A. M. López, *Eur. J. Inorg. Chem.*, 2021, 4731–4761; (*b*) R. Bai, X. Meng, X. Wang and L. He, *Adv. Funct. Mater.*, 2020, **30**, 1907169.

6 (*a*) S. Huo, J. Carroll and D. A. K. Vezzu, *Asian J. Org. Chem.*, 2015, **4**, 1210–1245; (*b*) Z. Feng, Y. Sun, X. Yang and G. Zhou, *Chem. Rec.*, 2019, **19**, 1710–1728; (*c*) M. Yoshida and M. Kato, *Coord. Chem. Rev.*, 2020, **408**, 213194.

7 (*a*) F. Barigelletti, D. Sandrini, M. Maestri, V. Balzani, A. Von Zelewsky, L. Chassot, P. Jolliet and U. Maeder, *Inorg. Chem.*, 1988, **27**, 3644–3647; (*b*) M. La Deda, A. Crispini, I. Aiello, M. Ghedini, M. Amati, S. Belviso and F. Lelj, *Dalton Trans.*, 2011, **40**, 5259–5270; (*c*) E. Anger, M. Rudolph, L. Norel, S. Zrig, C. Shen, N. Vanthuyne, L. Toupet, J. A. G. Williams, C. Roussel, J. Autschbach, J. Crassous and R. Réau, *Chem. – Eur. J.*, 2011, **17**, 14178–14198; (*d*) J. E. Expósito, M. Álvarez-Paino, G. Aullón, J. A. Miguel and P. Espinet, *Dalton Trans.*, 2015, **44**, 16164–16176; (*e*) X.-P. Zhang, F.-Q. Liu, J.-C. Lai, C.-H. Li, A.-M. Li and X.-Z. You, *New J. Chem.*, 2016, **40**, 2628–2636; (*f*) S. W. Thomas, K. Venkatesan, P. Müller and T. M. Swager, *J. Am. Chem. Soc.*, 2006, **128**, 16641–16648; (*g*) D. M. Jenkins and S. Bernhard, *Inorg. Chem.*, 2010, **49**, 11297–11308; (*h*) F. Juliá, M.-D. García-Legaz, D. Bautista and P. González-Herrero, *Inorg. Chem.*, 2016, **55**, 7647–7660; (*i*) F. Juliá, D. Bautista and P. González-Herrero, *Chem. Commun.*, 2016, **52**, 1657–1660; (*j*) F. Juliá and P. González-Herrero, *J. Am. Chem. Soc.*, 2016, **138**, 5276–5282; (*k*) F. Juliá and P. González-Herrero, *Dalton Trans.*, 2016, **45**, 10599–10608; (*l*) F. Juliá, D. Bautista, J. M. Fernández-Hernández and P. González-Herrero, *Chem. Sci.*, 2014, **5**, 1875–1880; (*m*) J. C. López-López, D. Bautista and P. González-Herrero, *Chem. – Eur. J.*, 2020, **26**, 11307–11315; (*n*) Á. Vivancos, D. Bautista and P. González-Herrero, *Chem. – Eur. J.*, 2019, **25**, 6014–6025; (*o*) F. Juliá, G. Aullón, D. Bautista and P. González-Herrero, *Chem. – Eur. J.*, 2014, **20**, 17346–17359.

8 (*a*) I. Maisuls, C. Wang, M. E. Gutierrez Suburu, S. Wilde, C.-G. Daniliuc, D. Brünink, N. L. Doltsinis, S. Ostendorp, G. Wilde, J. Kösters, U. Resch-Genger and C. A. Strassert, *Chem. Sci.*, 2021, **12**, 3270–3281; (*b*) M. Krause, R. von der Stück, D. Brünink, S. Buss, N. L. Doltsinis, C. A. Strassert and A. Klein, *Inorg. Chim. Acta*, 2021, **518**, 120093; (*c*) P.-K. Chow, W.-P. To, K.-H. Low and C.-M. Che, *Chem. – Asian J.*, 2014, **9**, 534–545.

9 (*a*) R. Malmberg and K. Venkatesan, *Coord. Chem. Rev.*, 2021, **449**, 214182; (*b*) M.-C. Tang, M.-Y. Chan and V. W.-W. Yam, *Chem. Rev.*, 2021, **121**, 7249–7279; (*c*) R. Bonsignore, S. R. Thomas, W. T. Klooster, S. J. Coles, R. L. Jenkins, D. Bourissou, G. Barone and A. Casini, *Chem. – Eur. J.*, 2020, **26**, 4226–4231.

10 (*a*) V. W.-W. Yam, K. M.-C. Wong, L.-L. Hung and N. Zhu, *Angew. Chem., Int. Ed.*, 2005, **44**, 3107–3110; (*b*) R. Malmberg, T. von Arx, M. Hasan, O. Blacque, A. Shukla, S. K. M. McGregor, S.-C. Lo, E. B. Namdas and K. Venkatesan, *Chem. – Eur. J.*, 2021, **27**, 7265–7274.

11 (*a*) J.-C. López-López, D. Bautista and P. González-Herrero, *Dalton Trans.*, 2021, **50**, 13294–13305; (*b*) Á. Vivancos, A. Jiménez-García, D. Bautista and P. González-Herrero, *Inorg. Chem.*, 2021, **60**, 7900–7913; (*c*) D. Poveda, Á. Vivancos, D. Bautista and P. González-Herrero, *Chem. Sci.*, 2020, **11**, 12095–12102.

12 (*a*) N. Giménez, R. Lara, M. T. Moreno and E. Lalinde, *Chem. – Eur. J.*, 2017, **23**, 5758–5771; (*b*) N. Giménez, E. Lalinde, R. Lara and M. T. Moreno, *Chem. – Eur. J.*, 2019, **25**, 5514–5526; (*c*) A. Corral-Zorzano, D. Gómez de Segura, E. Lalinde and M. T. Moreno, *Dalton Trans.*, 2023, **52**, 6543–6550.

13 (*a*) Y. Zhang, F. Meng, C. You, S. Yang, L. Xiong, W. Xiong, W. Zhu, Y. Wang, Y. Pei and S. Su, *Dyes Pigm.*, 2017, **142**, 457–464; (*b*) A. Ionescu, N. Godbert, I. Aiello, L. Ricciardi, M. La Deda, A. Crispini, E. Sicilia and M. Ghedini, *Dalton*

Trans., 2018, **47**, 11645–11657; (*c*) J. E. Expósito, G. Aullón, M. Bardají, J. A. Miguel and P. Espinet, *Dalton Trans.*, 2020, **49**, 13326–13338; (*d*) Y. M. Dikova, D. S. Yufit and J. A. G. Williams, *Inorg. Chem.*, 2023, **62**, 1306–1322.

14 Z. Yang, G. Jiang, Z. Xu, S. Zhao and W. Liu, *Coord. Chem. Rev.*, 2020, **423**, 213492.

15 X.-Q. Zhou, M. Xiao, V. Ramu, J. Hilgendorf, X. Li, P. Papadopoulou, M. A. Siegler, A. Kros, W. Sun and S. Bonnet, *J. Am. Chem. Soc.*, 2020, **142**, 10383–10399.

16 (*a*) A. P. King and J. J. Wilson, *Chem. Soc. Rev.*, 2020, **49**, 8113–8136; (*b*) P. Štarha, *Coord. Chem. Rev.*, 2021, **431**, 213690.

17 U. Das, B. Kar, S. Pete and P. Paira, *Dalton Trans.*, 2021, **50**, 11259–11290.

18 S. Pete, N. Roy and P. Paira, *Inorg. Chim. Acta*, 2021, **517**, 120184.

19 Y. Liu, Y. Wang, S. Song and H. Zhang, *Chem. Sci.*, 2021, **12**, 12234–12247.

20 (*a*) S. Dilruba and G. V. Kalayda, *Cancer Chemother. Pharmacol.*, 2016, **77**, 1103–1124; (*b*) C. Yu, Z. Wang, Z. Sun, L. Zhang, W. Zhang, Y. Xu and J.-J. Zhang, *J. Med. Chem.*, 2020, **63**, 13397–13412.

21 N. Nayeem and M. Contel, *Chem. – Eur. J.*, 2021, **27**, 8891–8917.

22 E. Ortega, G. Vigueras, F. J. Ballester and J. Ruiz, *Coord. Chem. Rev.*, 2021, **446**, 214129.

23 G.-X. Xu, E. C.-L. Mak and K. K.-W. Lo, *Inorg. Chem. Front.*, 2021, **8**, 4553–4579.

24 L. Feng, M. Gao, D. Tao, Q. Chen, H. Wang, Z. Dong, M. Chen and Z. Liu, *Adv. Funct. Mater.*, 2016, **26**, 2207–2217.

25 A. Khoury, K. M. Deo and J. R. Aldrich-Wright, *J. Inorg. Biochem.*, 2020, **207**, 111070.

26 (*a*) T. C. Johnstone, K. Suntharalingam and S. J. Lippard, *Chem. Rev.*, 2016, **116**, 3436–3486; (*b*) R. G. Kenny, S. W. Chuah, A. Crawford and C. J. Marmion, *Eur. J. Inorg. Chem.*, 2017, 1596–1612; (*c*) Z. Wang, Z. Deng and G. Zhu, *Dalton Trans.*, 2019, **48**, 2536–2544; (*d*) D. Gibson, *J. Inorg. Biochem.*, 2019, **191**, 77–84.

27 (*a*) E. Petruzzella, R. Sirota, I. Solazzo, V. Gandin and D. Gibson, *Chem. Sci.*, 2018, **9**, 4299–4307; (*b*) R. G. Kenny and C. J. Marmion, *Chem. Rev.*, 2019, **119**, 1058–1137; (*c*) H. Kostrhunova, E. Petruzzella, D. Gibson, J. Kasparkova and V. Brabec, *Chem. – Eur. J.*, 2019, **25**, 5235–5245; (*d*) C. Jia, G. B. Deacon, Y. Zhang and C. Gao, *Coord. Chem. Rev.*, 2021, **429**, 213640.

28 (*a*) C. Caporale and M. Massi, *Coord. Chem. Rev.*, 2018, **363**, 71–91; (*b*) S. Shaikh, Y. Wang, F. Ur Rehman, H. Jiang and X. Wang, *Coord. Chem. Rev.*, 2020, **416**, 213344; (*c*) B. Kar, N. Roy, S. Pete, P. Moharana and P. Paira, *Inorg. Chim. Acta*, 2020, **512**, 119858; (*d*) H. Shi, Y. Wang, S. Lin, J. Lou and Q. Zhang, *Dalton Trans.*, 2021, **50**, 6410–6417; (*e*) G. Millán, M. Nieddu, I. P. López, C. Ezquerro, J. R. Berenguer, I. M. Larráyoz, J. G. Pichel and E. Lalinde, *Dalton Trans.*, 2023, **52**, 6360–6374.

29 (*a*) N. Cutillas, G. S. Yellol, C. de Haro, C. Vicente, V. Rodríguez and J. Ruiz, *Coord. Chem. Rev.*, 2013, **257**, 2784–2797; (*b*) A. Kergreis, R. M. Lord and S. J. Pike, *Chem. – Eur. J.*, 2020, **26**, 14938–14946; (*c*) F. Guarra, A. Pratesi, C. Gabbiani and T. Biver, *J. Inorg. Biochem.*, 2021, **217**, 111355; (*d*) H. R. Shahsavari, J. Hu, S. Chamyani, Y. Sakamaki, R. B. Aghakhanpour, C. Salmon, M. Fereidoonnezhad, A. Mojaddami, P. Peyvasteh and H. Beyzavi, *Organometallics*, 2021, **40**, 72–82; (*e*) S. Garbe, M. Krause, A. Klimpel, I. Neundorf, P. Lippmann, I. Ott, D. Brünink, C. A. Strassert, N. L. Doltsinis and A. Klein, *Organometallics*, 2020, **39**, 746–756; (*f*) Q. Zhang, S. Wang, Y. Zhu, C. Zhang, H. Cao, W. Ma, X. Tian, J. Wu, H. Zhou and Y. Tian, *Inorg. Chem.*, 2021, **60**, 2362–2371; (*g*) Y. Zhang, Q. Luo, W. Zheng, Z. Wang, Y. Lin, E. Zhang, S. Lü, J. Xiang, Y. Zhao and F. Wang, *Inorg. Chem. Front.*, 2018, **5**, 413–424; (*h*) A. I. Solomatina, P. S. Chelushkin, T. O. Abakumova, V. A. Zhemkov, M. Kim, I. Bezprozvanny, V. V. Gurzhiy, A. S. Melnikov, Y. A. Anufrikov, I. O. Koshevoy, S.-H. Su, P.-T. Chou and S. P. Tunik, *Inorg. Chem.*, 2019, **58**, 204–217.

30 (*a*) Q. Zheng, X. Liu, Y. Zheng, K. W. K. Yeung, Z. Cui, Y. Liang, Z. Li, S. Zhu, X. Wang and S. Wu, *Chem. Soc. Rev.*, 2021, **50**, 5086–5125; (*b*) L. K. McKenzie, H. E. Bryant and J. A. Weinstein, *Coord. Chem. Rev.*, 2019, **379**, 2–29.

31 K. Qiu, Y. Chen, T. W. Rees, L. Ji and H. Chao, *Coord. Chem. Rev.*, 2019, **378**, 66–86.

32 Z. Xu, Z. Wang, Z. Deng and G. Zhu, *Coord. Chem. Rev.*, 2021, **442**, 213991.

33 (*a*) A. Lázaro, C. Balcells, J. Quirante, J. Badia, L. Baldomà, J. S. Ward, K. Rissanen, M. Font-Bardia, L. Rodríguez, M. Crespo and M. Cascante, *Chem. – Eur. J.*, 2020, **26**, 1947–1952; (*b*) M. Crespo, *J. Organomet. Chem.*, 2019, **879**, 15–26; (*c*) X. Su, B. Liu, W.-J. Wang, K. Peng, B.-B. Liang, Y. Zheng, Q. Cao and Z.-W. Mao, *Angew. Chem., Int. Ed.*, 2023, **62**, e202216917.

34 L. Hroch, L. Aitken, O. Benek, M. Dolezal, K. Kuca, F. Gunn-Moore and K. Musilek, *Curr. Med. Chem.*, 2015, **22**, 730–747.

35 (*a*) E. Lalinde, M. T. Moreno, R. Lara, I. P. López, E. Alfaro-Arnedo, J. G. Pichel and S. Piñeiro-Hermida, *Chem. – Eur. J.*, 2018, **24**, 2440–2456; (*b*) J. R. Berenguer, J. G. Pichel, N. Giménez, E. Lalinde, M. T. Moreno and S. Piñeiro-Hermida, *Dalton Trans.*, 2015, **44**, 18839–18855; (*c*) R. Lara, G. Millán, M. T. Moreno, E. Lalinde, E. Alfaro-Arnedo, I. P. López, I. M. Larráyoz and J. G. Pichel, *Chem. – Eur. J.*, 2021, **27**, 15757–15772.

36 N. Wang, M. Hu, S. K. Mellerup, X. Wang, F. Sauriol, T. Peng and S. Wang, *Inorg. Chem.*, 2017, **56**, 12783–12794.

37 (*a*) R. Corbo, D. C. Georgiou, D. J. D. Wilson and J. L. Dutton, *Inorg. Chem.*, 2014, **53**, 1690–1698; (*b*) A. N. Biswas, P. Das, V. Bagchi, A. Choudhury and P. Bandyopadhyay, *Eur. J. Inorg. Chem.*, 2011, 3739–3748.

38 (*a*) R. Malmberg, D. Suter, O. Blacque and K. Venkatesan, *Chem. – Eur. J.*, 2021, **27**, 14410–14417; (*b*) D. Gómez de Segura, R. Lara, M. Martínez-Junquera, E. Lalinde and M. T. Moreno, *Dalton Trans.*, 2022, **51**, 274–285.

39 M. C. DeRosa and R. J. Crutchley, *Coord. Chem. Rev.*, 2002, **233–234**, 351–371.

40 (*a*) F. Doettinger, Y. Yang, M. Karnahl and S. Tschierlei, *Inorg. Chem.*, 2023, **62**, 8166–8178; (*b*) R. Schmidt, C. Tanielian, R. Dunsbach and C. Wolff, *J. Photochem. Photobiol., A*, 1994, **79**, 11–17.

41 D.-F. Shi, T. D. Bradshaw, S. Wrigley, C. J. McCall, P. Lelieveld, I. Fichtner and M. F. G. Stevens, *J. Med. Chem.*, 1996, **39**, 3375–3384.

42 G. Millán, N. Giménez, R. Lara, J. R. Berenguer, M. T. Moreno, E. Lalinde, E. Alfaro-Arnedo, I. P. López, S. Piñeiro-Hermida and J. G. Pichel, *Inorg. Chem.*, 2019, **58**, 1657–1673.

43 G. Millán, M. Nieddu, I. P. López, C. Ezquerro, J. R. Berenguer, I. M. Larráyoz, J. G. Pichel and E. Lalinde, *Dalton Trans.*, 2023, **52**, 6360–6374.

44 (*a*) G. I. Davou, N. J. Chuwang, U. C. Essien, T. P. P. Choji, B. C. Echeonwu and M. D. Lugos, *Int. Res. J. Med. Med. Sci.*, 2019, **7**, 40–47; (*b*) J. Chen, J. Wang, Y. Deng, T. Wang, T. Miao, C. Li, X. Cai, Y. Liu, J. Henri and L. Chen, *Bioinorg. Chem. Appl.*, 2020, **2020**, 8890950; (*c*) M. S. Costa, Y. G. Gonçalves, B. C. Borges, M. J. B. Silva, M. K. Amstalden, T. R. Costa, L. M. G. Antunes, R. S. Rodrigues, V. de Melo Rodrigues and E. de Faria Franca, *Sci. Rep.*, 2020, **10**, 1–21.

45 (*a*) R. B. Badisa, S. F. Darling-Reed, P. Joseph, J. S. Cooperwood, L. M. Latinwo and C. B. Goodman, *Anticancer Res.*, 2009, **29**, 2993–2996; (*b*) J. A. Valderrama, V. Delgado, S. Sepúlveda, J. Benites, C. Theoduloz, P. Buc Calderon and G. G. Muccioli, *Molecules*, 2016, **21**, 1199.

46 (*a*) C. Li, K.-W. Ip, W.-L. Man, D. Song, M.-L. He, S.-M. Yiu, T.-C. Lau and G. Zhu, *Chem. Sci.*, 2017, **8**, 6865–6870; (*b*) P. W. Prasetyaningrum, A. Bahtiar and H. Hayun, *Sci. Pharm.*, 2018, **86**, 25–37; (*c*) N. Pantelić, B. B. Zmejkovski, D. D. Marković, J. M. Vujić, T. P. Stanojković, T. J. Sabo and G. N. Kaluđerović, *Metals*, 2016, **6**, 226.

47 (*a*) Y. Wu, S. Li, Y. Chen, W. He and Z. Guo, *Chem. Sci.*, 2022, **13**, 5085–5106; (*b*) C.-P. Tan, Y.-M. Zhong, L.-N. Ji and Z.-W. Mao, *Chem. Sci.*, 2021, **12**, 2357–2367; (*c*) J. Li and T. Chen, *Coord. Chem. Rev.*, 2020, **418**, 213355.

48 (*a*) C. Wang, L. Lystrom, H. Yin, M. Hetu, S. Kilina, S. A. McFarland and W. Sun, *Dalton Trans.*, 2016, **45**, 16366–16378; (*b*) J. Pracharova, G. Vigueras, V. Novohradsky, N. Cutillas, C. Janiak, H. Kostrhunova, J. Kasparkova, J. Ruiz and V. Brabec, *Chem. – Eur. J.*, 2018, **24**, 4607–4619; (*c*) L. C.-C. Lee, A. W.-Y. Tsang, H.-W. Liu and K. K.-W. Lo, *Inorg. Chem.*, 2020, **59**, 14796–14806.

49 J. Yellol, S. A. Pérez, A. Buceta, G. Yellol, A. Donaire, P. Szumlas, P. J. Bednarski, G. Makhloufi, C. Janiak, A. Espinosa and J. Ruiz, *J. Med. Chem.*, 2015, **58**, 7310–7327.

50 (*a*) M. Frik, J. Jimenez, V. Vasilevski, M. Carreira, A. de Almeida, E. Gascon, F. Benoit, M. Sanau, A. Casini and M. Contel, *Inorg. Chem. Front.*, 2014, **1**, 231–241; (*b*) G. Cohen, W. Bauer, J. Barton and S. Lippard, *Science*, 1979, **203**, 1014–1016; (*c*) M. Martínez-Junquera, E. Lalinde, M. T. Moreno, E. Alfaro-Arnedo, I. P. López, I. M. Larráyoz and J. G. Pichel, *Dalton Trans.*, 2021, **50**, 4539–4554.